Proceedings of 2004 IEEE/RSJ International Conference on Intelligent Robots and Systems
September 28 - October 2, 2004, Sendai, Japan

Load Distribution Algorithms and Experimentation For a Redundantly Actuated, Singularity-Free 3-DOF Parallel Haptic Device

Tae-Ju Kim
Division for Applied Robot Technology (DART)
Korea Institute of Industrial Technology (KITECH)
Chunan & Ansan, Korea
remember94@empal.com

Byung-Ju Yi
School of Electrical Engineering and Computer Science
Hanyang University
Ansan, Korea
bj@hanyang.ac.kr

Il Hong Suh
School of Information and Communication
Hanyang University
Seoul, Korea
ihsuh@hanyang.ac.kr

***Abstract*—Parallel-type mechanisms provide many advantages over serial-type mechanisms. However, in case of using parallel structures as a haptic device, it is sometimes hard to ensure the performance of the force reflection due to many singular points existing in workspace. In this paper, we propose a redundantly actuated parallel 3-DOF haptic device, which is singularity-free in the workspace and also has an improved force reflection capability. Using two sets of actuators with different size and different force resolution, we propose several useful load distribution algorithms considering force resolution and torque limit. We confirm the performance of the force reflection capability throughout simulation and experimentation.**

Keywords- Parallel Mechanism, Redundant Actuation, Haptic, Load Distribution, Force Reflection

I. INTRODUCTION

General requirement of haptic devices includes large workspace and enough reflection force for human operator, low apparent mass/inertia, low friction, high structural stiffness, backdriveability, absence of mechanical singularities, compactness, and so on. [1,2]. Parallel structures have been proposed as a potential application of the haptic device because of their compact structure, high force and stiffness, and high accuracy. However, multiple singular points existing inside the workspace makes real implementation difficult [3]. To cope with this problem, utilization of redundant actuation has been suggested as a solution.

Redundant actuation can be easily explained in terms of mobility. Mobility of a system is defined as the number of minimum parameters, which is required to specify all the locations of the system relative to another. And it is described by

$$M = D(L-1) - \sum_{i=1}^{j} (D - F_i) \qquad (1)$$

where D, L, F_i, and J denote the maximum motion degree of link, the number of link, the motion degree of i th joint, and the number of joint, respectively. When the number of actuators of the system is greater than M, the system is called a redundantly actuated system. Redundant actuation provides general improvement in payload, maximum velocity and acceleration. More importantly, the surplus actuators play a role of avoiding the singularity by abundant sources existing in the column space that relates the joint actuators to the output forces [7]. Furthermore, the force redundancy allows several optimization algorithms, which can be exploited to enhance the performances of the haptic device.

In this paper, we propose methodologies for singularity-free load distribution and simultaneous generation of coarse and fine reflection force to improve the performance of haptic devices. For this, we employ two sets of actuators ; a base actuator set and a floating actuator set with different actuator size. The base actuator has high power but coarse force resolution. The floating actuator has fine force resolution but low power. The basic concept of this algorithm is to increase the payload and to preserve fine force resolution by using two sets of actuators with different size and accuracy. Generally an actuator with high power and high force resolution is very expensive. Instead of employing such expensive actuators in the design of haptic device, it is possible to deliver the same effect with less cost by using two sets of actuator. Using the surplus number of actuators, we propose several load distribution algorithms to achieve this purpose and also to resolve the torque saturation problem.

II. KINEMATICS OF 3-DOF HAPTIC DEVICE

A. Geometric Description

The haptic device proposed in this paper consists of a top plate and three serial chains connecting the top plate to the six actuators, as shown in Fig. 1. One set of three actuators are placed at the base and the other set of actuators are attached to the every second joint of the mechanism. Each of the three serial chains consists of three links and three revolute joints. The length of every link is $0.1m$, and the base joint of each of the three chains is placed on the circle of radius (R) with 120° apart from each other.

This study was supported by a grant of the Korea Health 21 R&D Project Ministry of Health & Welfare, Republic of Korea.(02-PJ3-PG6-EV04-0003)

0-7803-8463-6/04/$20.00 ©2004 IEEE

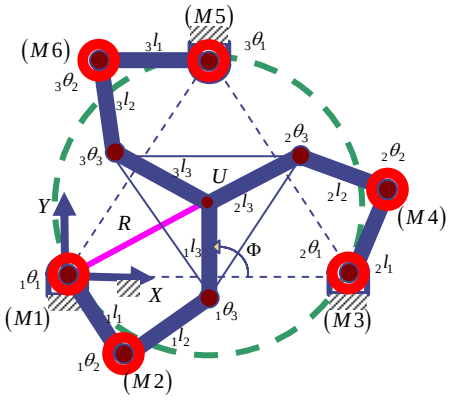

Figure 1. 3-DOF Parallel Haptic Device

B. *Forward Kinematics*

The solution of forward kinematics for each serial chain is described as

$$\underline{u} = \begin{bmatrix} {}_1l_3\,{}_1C_{123} + {}_1l_2\,{}_1C_{12} + {}_1l_1\,{}_1C_1 \\ {}_1l_3\,{}_1S_{123} + {}_1l_2\,{}_1S_{12} + {}_1l_1\,{}_1S_1 \\ {}_1\theta_1 + {}_1\theta_2 + {}_1\theta_3 \end{bmatrix}$$

$$= \begin{bmatrix} {}_2l_3\,{}_2C_{123} + {}_2l_2\,{}_2C_{12} + {}_2l_1\,{}_2C_1 + R\sqrt{3} \\ {}_2l_3\,{}_2S_{123} + {}_2l_2\,{}_2S_{12} + {}_2l_1\,{}_2S_1 \\ {}_2\theta_1 + {}_2\theta_2 + {}_2\theta_3 \end{bmatrix}, \qquad (2)$$

$$= \begin{bmatrix} {}_3l_3\,{}_3C_{123} + {}_3l_2\,{}_3C_{12} + {}_3l_1\,{}_3C_1 + \dfrac{R\sqrt{3}}{2} \\ {}_3l_3\,{}_3S_{123} + {}_3l_2\,{}_3S_{12} + {}_3l_1\,{}_3S_1 + \dfrac{3R}{2} \\ {}_3\theta_1 + {}_3\theta_2 + {}_3\theta_3 \end{bmatrix}$$

where ${}_i\theta_j$ denotes the j th joint angle of the i th chain.

In the following, we describe the relationship between the operational velocity ($\dot{\underline{u}}$) and the all joint actuators' velocity ($\dot{\underline{\theta}}$). Differentiating (2) with respect to time gives the velocity relation

$$\dot{\underline{u}} = \left[{}_1G_\phi^u\right]{}_1\dot{\underline{\phi}} = \left[{}_2G_\phi^u\right]{}_2\dot{\underline{\phi}} = \left[{}_3G_\phi^u\right]{}_3\dot{\underline{\phi}}, \qquad (3)$$

where

$$\left[{}_iG_\phi^u\right] = \begin{bmatrix} \dfrac{\partial u}{\partial_i\phi_1} & \dfrac{\partial u}{\partial_i\phi_2} & \dfrac{\partial u}{\partial_i\phi_3} \end{bmatrix} = \left[{}_ig_1 \;\; {}_ig_2 \;\; {}_ig_3\right]. \qquad (4)$$

and

$${}_i\dot{\underline{\phi}} = \left[{}_i\dot{\theta}_1 \quad {}_i\dot{\theta}_2 \quad {}_i\dot{\theta}_3\right]^T. \qquad (5)$$

By choosing the every base joint and every second joint (i.e., ${}_1\dot{\theta}_1$, ${}_1\dot{\theta}_2$, ${}_2\dot{\theta}_1$, ${}_2\dot{\theta}_2$, ${}_3\dot{\theta}_1$ and ${}_3\dot{\theta}_2$) as the active joints set ($\dot{\underline{\phi}}_A$), we have a relationship between the active joints and the velocity of the end-effector :

$$\dot{\underline{\phi}}_A = \left[G_u^A\right]\dot{\underline{u}}, \qquad (6)$$

where

$$\left[G_u^A\right] = \left[\left[{}_1G_u^\phi\right]_{1;}\left[{}_1G_u^\phi\right]_{2;}\left[{}_2G_u^\phi\right]_{1;}\left[{}_2G_u^\phi\right]_{2;}\left[{}_3G_u^\phi\right]_{1;}\left[{}_3G_u^\phi\right]_{2;}\right]^T, \qquad (7)$$

and

$$\dot{\underline{\phi}}_a = \left[{}_1\dot{\underline{\theta}}_1 \quad {}_2\dot{\underline{\theta}}_1 \quad {}_3\dot{\underline{\theta}}_1\right]. \qquad (8)$$

$\left[{}_iG_u^\phi\right]_{j;}$ denotes the j-*th* row of the inverse Jacobian for the i-*th* chain.

According to the duality existing between the velocity vector and the force vector, the force relationship between the actuator space and the joint input space is given by

$$\underline{T}_u = \left[G_u^A\right]^T\underline{T}_A\ , \qquad (9)$$

where $\underline{T}_u \in R^3$ denotes the output force vector and $\underline{T}_A \in R^6$ denotes the joint torque vector.

III. LOAD DISTRIBUTION ALGORITHMS

The proposed 3-DOF haptic mechanism is driven by 6 actuators; three on the base location and three on the second joint location. This redundant architecture provides general improvement in payload, maximum velocity and acceleration. More importantly, the surplus actuators play a role of avoiding the singularity by abundant sources existing in the column space that relates the joint actuators to the output forces. Furthermore, the force redundancy allows several optimization algorithms, which can be exploited to enhance the performances of the haptic device. The basic concept of this algorithm is to increase the payload and to preserve fine force resolution by using two sets of actuators with different size and accuracy. Generally an actuator with high power and high force resolution is very expensive. Instead of employing such expensive actuators in the design of haptic device, it is possible to deliver the same effect with less cost by using two sets of actuator; one has high power with low accuracy and the other has low power with high accuracy. We select the base actuators as high power device with coarse force resolution because it is rather heavy, and the floating actuators are on the reverse. Based on this actuator architecture, we propose several useful load distribution algorithms.

A. *Weighted Pseudo-inverse Solution*

The general solution of (9) is given by

$$\underline{T}_A = \left(\left[G_u^A\right]^T\right)^+\underline{T}_u + \left(I - \left(\left[G_u^A\right]^T\right)^+\left(\left[G_u^A\right]^T\right)\right)\underline{\varepsilon}. \qquad (10)$$

In order to reflect force or torque having both high and low force-resolution, the force or torque felt in the operational position should be distributed to the base and floating actuators according to some fashion. Using a weighted pseudo-inverse is one way. The weighted pseudo-inverse is given by

$$\left(\left[G_u^A\right]^T\right)^+ = [W]^{-1}\left[G_u^A\right]\left(\left[G_u^A\right]^T[W]^{-1}\left[G_u^A\right]\right)^{-1}, \qquad (11)$$

where

$$[W] = diag\{w_1, w_2, w_3, w_4, w_5, w_6\}. \qquad (12)$$

The magnitude of weighting factors can be decided according to the size of actuators. For instance, the weighting factors for the base actuators and the floating actuator can be given as

$$w_{1,3,5} = K_1,\ w_{2,4,6} = K_2, \tag{13}$$

where K_1 and K_2 denote the scaling factors.[6] The weighting factor for the base actuators is given smaller than that for the floating actuators so that the operational force and torque distributed to the base actuators should be larger than those distributed to the floating actuators. The magnitude of the weighting factor is given proportional to square of the actuator size since the performance index for the pseudo-inverse solution is the sum of product of each weighting factor and the square of each actuator's torque.

B. Sub-criteria Using the Null-space Solution

1) Load distribution algorithm using two sets of actuators having different sizes and force resolutions

The null-space solution can be utilized for several sub-criteria. Here, we propose load distribution algorithms that consider the actuator saturation and resolution. High reflection-force and fine force-resolution are desirable for effective haptic application. However, both functions cannot be met with one single actuator. Thus, we select the base actuator as a high power actuator with coarse force resolution, and the floating actuator as one having low power and high force-resolution. This actuator architecture simultaneously allows high force reflection as well as fine force resolution.

A load distribution algorithm is introduced, which deals with the fine force resolution. The null-space is exploited to employ this algorithm. A special constraint relation given by [4,6]

$$\underline{T}_{Base} = [K]\underline{T}_A \tag{14}$$

is employed to install this objective. Here, $\underline{T}_{Base} \in R^3$, $\underline{T}_A \in R^6$, and $[K] \in R^{3x6}$ are given as

$\underline{T}_{Base} = (T_1 - R_B, T_3 - R_B, T_5 - R_B)^T, \underline{T}_A = (T_1, T_2, T_3, T_4, T_5, T_6)^T$

and

$$[K] = \begin{bmatrix} 1 & 0 & 0 & 0 & 0 & 0 \\ 0 & 0 & 1 & 0 & 0 & 0 \\ 0 & 0 & 0 & 0 & 0 & 1 \end{bmatrix}.$$

$[K]$ is a selection matrix that only chooses the base actuators, and the components of $\underline{T}_{Base}$ imply the modification of the amount of each base actuator's torque. It is obtained by subtracting the given magnitude of force resolution from the each base actuator's torque of the pseudo-inverse solution. Thus, substituting (10) into (14) yields

$$\begin{aligned} \underline{T}_{Base} &= [K]\underline{T}_A = [K]\left(\left[G_u^A\right]^T\right)^+ \underline{T}_u \\ &+ [K]\left(I - \left(\left[G_u^A\right]^T\right)^+ \left(\left[G_u^A\right]^T\right)\right)\underline{\varepsilon}\,. \end{aligned} \tag{15}$$

By rearranging (15), we can decide the null-space vector $\underline{\varepsilon}$ and the final form of the solution is obtained as

$$\underline{T}_A = \left(\left[G_u^A\right]^T\right)^+ \underline{T}_u + [B]^+ \left(\underline{T}_{Base} - [K]\left(\left[G_u^A\right]^T\right)^+ \underline{T}_u\right). \tag{16}$$

where

$$[B] = \left([K]\left(I - \left(\left[G_u^A\right]^T\right)^+ \left(\left[G_u^A\right]^T\right)\right)\right). \tag{17}$$

The solution given by (16) redistributes the actuator torques such that the large base-actuators take on the role of generating large actuator torques and the small, floating actuators take on the role of controlling fine forces. Another good point of employing small actuators on the floating joints is that it can minimize the inertial force carried by the floating actuators.

2) Load distribution algorithm considering torque limit

Now, we consider the case that some of the actuators are over-actuated as the result of the pseudo-inverse solution. In this case, the system load should be redistributed such that the saturated joint is confined to generate its maximum torque and the other joints take the burden given to the saturated joints. Similar to (14), we can decide $\underline{T}_{Base}$ and $[K]$ that corresponds to this purpose.

Assuming that the i th floating actuator is over the torque limit, we can set the torque of the saturated joint as a fixed value and then distribute the burden to the other actuators [5]. It can be done by employing

$$[G_1]\underline{T}_A = T_{\max}, \tag{18}$$

where $[G_1]$ is a vector in which the i th element is 1, and the others are 0 and $T_{\max}$ is the maximum actuator size.

Substituting (10) into (18) yields the following equation

$$T_{\max} = [G_1]^T \underline{T}_A = [G_1]\begin{pmatrix} \left(\left[G_u^A\right]^T\right)^+ \underline{T}_u \\ +\left(I - \left(\left[G_u^A\right]^T\right)^+ \left(\left[G_u^A\right]^T\right)\right)\underline{\varepsilon} \end{pmatrix}. \tag{19}$$

Therefore, the vector $\underline{\varepsilon}$ can be obtained as

$$\underline{\varepsilon} = [C]^+ \left(T_{\max} - [G_1]\left(\left[G_u^A\right]^T\right)^+ \underline{T}_u\right) + \left([I] - [C]^+ [C]\right)\varepsilon_1, \tag{20}$$

where

$$[C] = [G_1]\left(I - \left(\left[G_u^A\right]^T\right)^+ \left(\left[G_u^A\right]^T\right)\right).$$

Substituting (20) into (10) yields a new solution, which takes into account the torque limit

$$\begin{aligned} \underline{T}_A = &\left(\left[G_u^A\right]^T\right)^+ \underline{T}_u + [C]^+ \left(T_{\max} - [G_1]\left(\left[G_u^A\right]^T\right)^+ \underline{T}_u\right) \\ &+ \left([I] - [C]^+ [C]\right)\varepsilon_1. \end{aligned} \tag{21}$$

3) Combination of sub-criteria

The additional null-space of (21) can be also exploited for additional sub-tasks. Here, we propose a load distribution algorithm that combines the two previous criteria. Assuming that only one redundant degree was employed to resolve the torque saturation, then the other two null-space dimensions can be utilized for other purposes. For example, the algorithm based on the two sets of actuators can be incorporated.

This scenario can be achieved by substituting (21) into the constraint form given by (14). The remaining degrees (i.e., two

floating actuators) will participate to this process. Thus, we have $\underline{T}_{Base} \in R^2$ and $[K] \in R^{2x6}$.

Thus, the final solution is obtained as

$$\underline{T}_A = \left(\left[G_u^A\right]^T\right)^+ \underline{T}_u + [C]^+ \left(\underline{T}_{\max} - [G_1]\left(\left[G_u^A\right]^T\right)^+ \underline{T}_u\right) + [D]^+ \left(\underline{T}_{Base} - [G_2]\left(\begin{array}{l}\left(\left[G_u^A\right]^T\right)^+ \underline{T}_u \\ + [C]^+ \left(\underline{T}_{\max} - [G_1]\left(\left[G_u^A\right]^T\right)^+ \underline{T}_u\right)\end{array}\right)\right). \quad (22)$$

where

$$[D] = [G_2]\left(I - [C]^+[C]\right).$$

This solution implies that it avoids the torque saturation of some floating actuator as well as achieves fine force generation by redistributing the actuator loads.

IV. Simulation Result

A simulator consists of a virtual rectangular wall having elasticity as shown in Fig. 2(a). The wall restricts the motion of the moving object. A virtual object is operated by the user's command from the haptic device. When collision between the object and the wall occurs, the reflecting force can computed. This simulation is performed by using Visual C++ 6.0 with OpenGL on the Windows NT environment. The haptic device generates a reflecting force according to the situation of virtual environment. Collision between the object and the environment generates some reflection force. Several load distribution algorithms to compute actuator torque are tested and compared in this section.

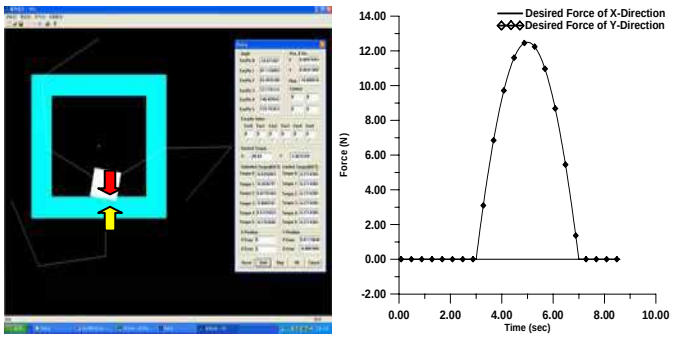

(a) Virtual simulation (b) Desired output force (T_u)

Figure 2. Simulation Environment

A. Comparison of Minimum Norm Solution and Weighted Pseudo-Inverse Solution

When a moving object collides with the wall, the reflecting force to restrict the operator's motion has to be generated. Fig. 2(b) illustrates the desired force profile to be generated at the operational task position. Specifically, Fig. 3(a) shows the torque profile of a base actuator (M5; line with point) and a floating actuator (M6; solid line) to satisfy the reflecting force that is given in Fig. 2(b). This solution is computed from the first term of (10), where the weighting matrix is given an identity matrix. Refer to Fig. 1 for the name of actuators.

Though this solution shows the minimum torque norm, a high torque is observed at the floating actuator (M6) having a small actuator size, which may cause torque saturation at the floating actuator (M6). For more efficient distribution of actuating torque, the weighted pseudo-inverse algorithm is employed. Using this algorithm, the base actuator (M5) takes on large torque and the floating actuator (M6) takes on smaller torque to avoid saturation.

Fig. 3(b) illustrates the torque calculated by using weighed pseudo inverse. It can be seen that the torque of the floating actuator becomes smaller, enough to avoid saturation. Thus, the weighted pseudo-inverse algorithm can be used as an effective means to avoid saturation.

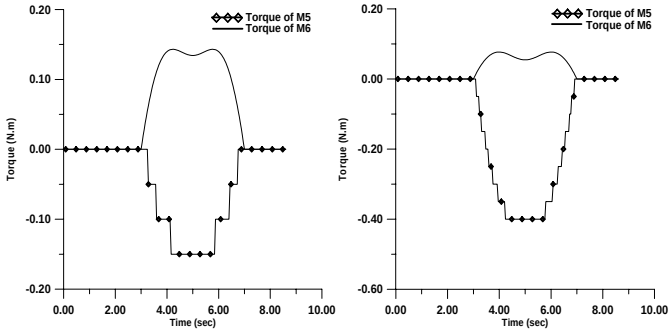

(a) (b)

Figure 3. Torque values of actuator M5 and M6

B. Comparison of Weghted Pseudo-Inverse Solution and Load distribution Algorithm For Generating Fine Force

Even when employing the weighted pseudo inverse algorithm, the output reflecting force still may not be accurate because of the coarse resolution of the base actuators. Here, we assume that the base actuators (M1, M3, M5) can not generate the force that is below 0.05 Nm.

Based on the pseudo-inverse algorithm, Fig. 4(a) shows the torque profiles of a base actuator (M1) and a floating actuator (M2) to satisfy the reflecting force that is given by Fig. 2(b). On the other hands, Fig. 4(b) shows the actuator torques for M1 and M2 when employing the fine force resolution algorithm. As shown in this plot, the value of the floating actuator is fluctuating to compensate for the inaccurate output force due to the coarse base actuators. When employing the weighted pseudo-inverse algorithm, the output force profile given in Fig. 5(a) shows an inaccurate force resolution. Both y- and x-directional forces are shown to be inaccurate.

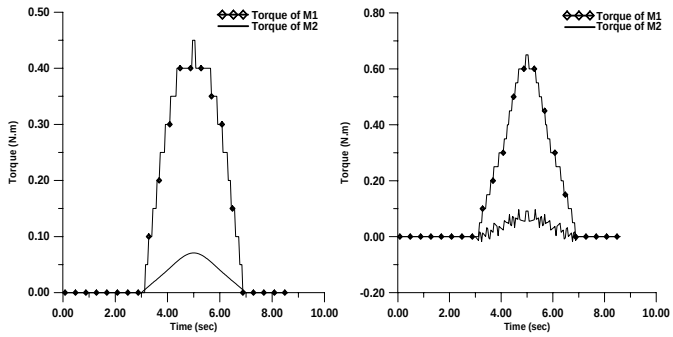

(a) (b)

Figure 4. Torque values of actuator M1 and M2

On the other hand, as shown in Fig. 5(b), the algorithm given in (16) employing fine actuators at the floating joints yields a better profile, which is almost the same as the planned output force given in Fig. 2(b).

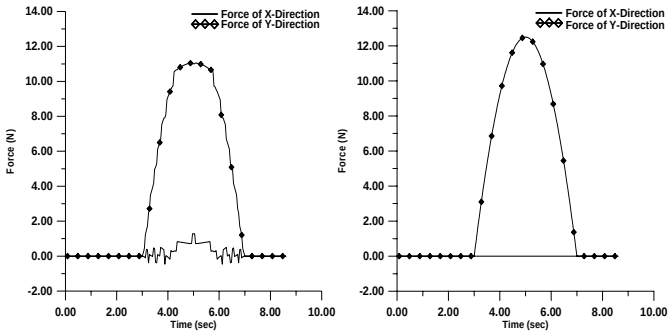

(a) Weighted pseudo-inverse (b) Precision force

Figure 5. Output force profiles

C. Comparison of Weghted Pseudo-Inverse Solution and Load distribution Algorithm with Consideration of Torque Limit

Even when employing the weighted pseudo inverse algorithm, some of the small-sized floating actuators still can be saturated. In this case, we can set the torque of the floating actuator as a fixed value and distributes the burden to the other actuators by using the null-space. Fig. 6(a) illustrates the torque of a base actuator (M3) and a floating actuator (M4) for the weighted pseudo-inverse algorithm. Despite of employing the weighted pseudo inverse, this case shows that the torque of floating actuator is over the torque limit. (for instance, $0.3Nm$)

To resolve this problem, the null-space solution given in (21) is employed. It is shown in Fig. 6(b) that when the maximum torque of the floating actuator is fixed as $0.3N.m$, the burden is distributed to the other actuators without any additional torque saturation. Thus, redistribution of the system load by using the null-space is effective to ensure avoidance of torque saturation along with satisfying the desired reflecting force at the end-position

D. Comparison of Load distribution Algorithm with Consideration of Torque Limit and Load distribution Algorithm with Consideration of Torque Limit and Precision Force

As an extension of the torque limit algorithm, it is still necessary to realize a precision force because of the coarse resolution of the base actuators. It can be also achieved by using the additional null-space solution given in (22).

Fig. 7 represents the torque values of the base actuator (M3) and the floating actuator (M4) for the algorithm considering both the torque limit and precision force. As shown in Fig. 7, M4 fluctuates a little to compensate for the inaccurate force resolution of the coarse base actuators.

Fig. 8(a) and Fig. 8(b) represent the output forces for the torque limit algorithm and the load distribution algorithm with consideration of both torque limit and precision force, respectively. Figure 8(b) shows that the Y-directional force is close to the desired output force and the unwanted X-directional force is removed. Some fluctuation is due to only employing two redundancies, instead of full redundancies. However, the output force is still satisfactory.

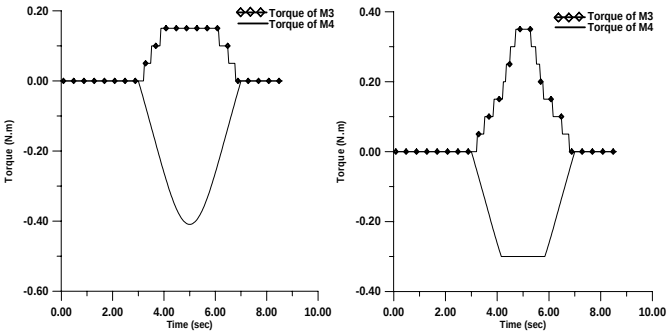

(a) (b)

Figure 6. Torque values of actuator M3 and M4

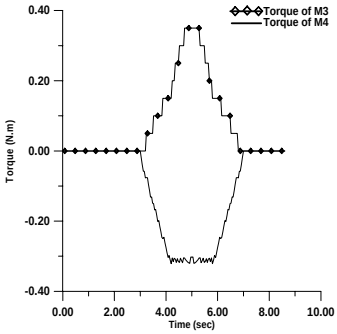

Figure 7. Torque values of actuator M3 and M4

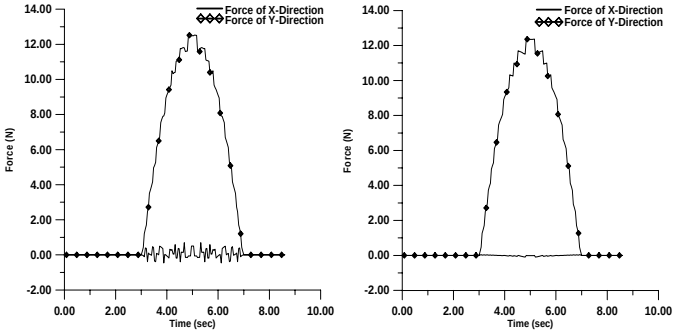

(a) Torque limit (b) Torque limit and precision force

Figure 8. Output Force Using Load distribution Algorithms

Figure 9. Prototype of 3 DOF parallel haptic device

Figure 10. Hinge Structure

V. EXPERIMENTATION

Fig. 9 shows a 3 DOF parallel haptic device developed for experimental verification. In order to measure the desired output force, a 6 DOF force/torque sensor is fixed to the ground frame, and the output position of the haptic device is connected to the sensor. Then, using a virtual spring model along the direction perpendicular to the sensor surface, a linear motion is executed so that a force profile similar to Fig. 2(b) can be measured. Fig. 10 shows a hinge structure, a wire and gear reduction system to achieve high force reflection along with soft feeling. Fig. 11 shows the experimental results of the proposed load distribution algorithms. Fig. 11(b) exhibits the best force reflection, which is almost the same as the desired force history given in Fig. 2(b). This is the case employing precision force-resolution algorithm introduced in Eq. (16). On the other hand, the weighted pseudo-inverse algorithm given in Fig. 11(a) shows the worst force reflection performance. The overall trend of the experimental results is similar to that of the simulation result. The inherent noise of the force/torque sensor is eliminated using a low-pass filter. The operator was able to distinguish the difference of reflecting forces.

VI. CONCLUSION

In this work, we proposed new load distribution algorithms in which reflecting force of both high and low resolution is achievable by using two sets of actuators with different size. Minimum norm solution, weighted pseudo inverse algorithm, a load distribution algorithm for precision force, and a load distribution algorithm considering torque limit are investigated. Using a redundantly actuated 3 DOF parallel haptic device, the performances of the proposed load distribution algorithms are verified throughout both simulation and experimentation.

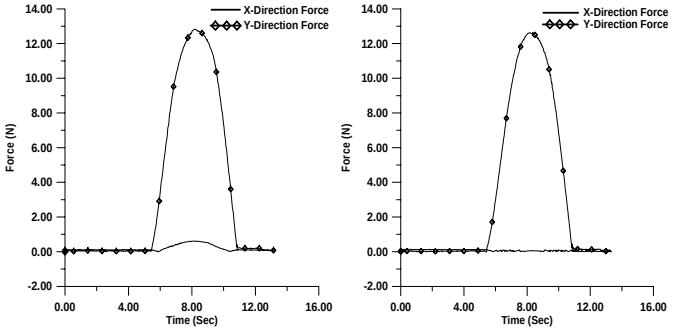

(a) Weighted pseudo-inverse (b) Precision force

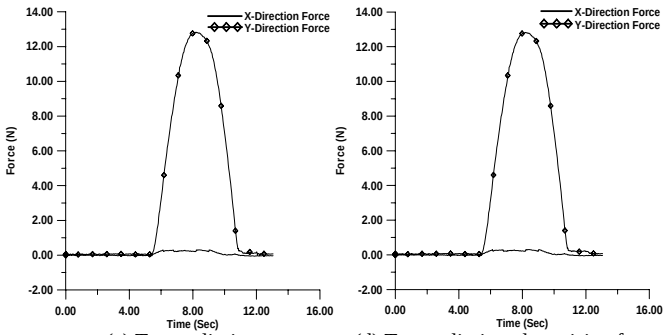

(c) Torque limit (d) Torque limit and precision force

Figure 11. Measurement of the output force for the proposed algorithms

REFERENCES

[1] Hyung Wook Kim, Jae Hoon Lee, Byung-Ju Yi and Il Hong Suh, "Design Scheme for a 6-DOF Parallel Haptic Device and Comparative Study on the Singularity-Free Algorithms," Journal of Control, Automation and Systems Engineering, Vol. 8, No. 12, pp. 1041-1047, 2002.

[2] R.E. Ellis, O.M. Ismaeil, and M.G. Lipsett, "Design and Evaluation of High-Performance Haptic Interface," *Robotica*, Vol. 4, 1996

[3] C. Gosselin, J. Angeles, "The Optimum Kinematic Design of a Planar Three-Degree-of-Freedom Parallel Manipulator," Journal of Mechanisms, Transmissions, and Automation in Design ,Vol. 110, pp. 35-41, 1988.

[4] J.M. Hollerbach and K.C. Suh, "Redundancy Resolution of Manipulators through Torque Optimization," Journal of Robotics and Automation , Vol. RA-3, No. 4, pp. 308-316, August 1987.

[5] Sang Heon Lee, "Control of Active Stiffness and Impact Disturbance by Redundancy Actuated Mechanism," Ph,D. Dissertation, Department of Mechanical Engineering, KAIST, 2000.

[6] Y. Nakamura, Advanced Robotics: Redundancy and Optimization, Addison-Wesley Publishing Company, 1991.

[7] Byung-Ju Yi, Sang-Rok Oh, and Il Hong Suh, "A Five-bar Finger Mechanism Involving Redundant Actuator : Analysis and Its Application," Journal of Robotics and Automation, Transaction of the IEEE, Vol. 15, No. 6, pp. 1001-1010, 1999.